A Prototype Smartwatch Utilizing Spectroscopy for Real-Time Monitoring of Hydration Status

Nazim A.Belabbaci

Submitted to Miner School of Computer & Information Sciences,
University of Massachusetts Lowell,

in partial fulfillment of the requirements for the degree of

Master of Science

February 2024

Computer Science Program

Signature Page

A Prototype Smartwatch Utilizing Spectroscopy for Real-Time Monitoring of Hydration Status

BY
NAZIM A.BELABBACI
B.S. INSTITUTE OF ELECTRICAL & ELECTRONICS OF ALGERIA (2017)
M.Eng. INSTITUTE OF ELECTRICAL & ELECTRONICS OF ALGERIA (2019)

SUBMITTED IN PARTIAL FULFILLMENT OF THE REQUIREMENTS
FOR THE DEGREE OF MASTER OF SCIENCE
COMPUTER SCIENCE
UNIVERSITY OF MASSACHUSETTS LOWELL

Signature of Author: DocuSigned by: Nazim Belabbaci 9BAB9E4BA4B74E5... Date: 11/22/2023

Signature of Thesis Supervisor: DocuSigned by: Arif 46163...FB23E64E2... Date: 11/22/2023

Name Typed: Mohammad Arif Ul Alam

Committee Member Signatures:

Committee Member Signature: DocuSigned by: Jerome Delhommelle 3E862D658C4D402... Typed Name: Jerome Delhommelle
Committee Member Signature: DocuSigned by: Hong Yu C97D8EFC3A014BE... Typed Name: Hong Yu
Committee Member Signature: _____ Typed Name: _____

A Prototype Smartwatch Utilizing Spectroscopy for Real-Time Monitoring of Hydration Status

BY
NAZIM A.BELABBACI

ABSTRACT OF A DISSERTATION SUBMITTED IN PARTIAL FULFILLMENT OF THE REQUIREMENTS

FOR THE DEGREE OF MASTER OF SCIENCE
COMPUTER SCIENCE
UNIVERSITY OF MASSACHUSETTS LOWELL
2024

Thesis Supervisor: Dr.Mohammad Arif Ul Alam
Assistant Professor, Department of Computer Science

Abstract

The demand for continuous health monitoring solutions has led to the development of innovative wearable biosensors. In this thesis, we introduce a novel approach to real-time hydration assessment using smartwatches equipped with a low-cost spectroscopy sensor. By integrating this technology into everyday a wearable, we aim to provide a convenient and non-invasive method for monitoring hydration levels based on blood electrolytes concentration.

We present two significant use cases: 1.the measurement of electrolyte solutions using our low-cost spectroscopy sensor and benchmark it with a high resolution spectrometer that follows industry standards. 2. the assessment of skin hydration during workout and fasting experiments. These use cases demonstrate the credibility of the proposed system.

We describe the signal processing techniques we used to extract meaningful data from spectroscopic measurements. Additionally, an AI algorithm is implemented on the edge, allowing real-time classification of hydration status into 3 distinct classes.

In the results evaluation section, we present the findings of our research, showcasing the system's accuracy and performance in assessing hydration status. We also delve into additional results, focusing on emotion recognition. For this purpose, a dedicated experimental setup is described, involving the use of spectroscopy data to develop an algorithm to classify emotions as sad or happy.

In conclusion, our thesis underscores the significance of smartwatch-based electrolyte measurement for real-time hydration assessment and its potential applications in diverse areas of health monitoring. We discuss the implications of our findings and suggest future work that can further enhance this technology's capabilities.

Contents

1 Introduction

Water is a fundamental component of the human body, constituting around 60 of an adult's total body mass and playing a pivotal role in the functioning of various organs. This indispensability of water underscores the importance of maintaining proper hydration levels for overall health and well-being(1). Ironically, both underhydration and overhydration pose risks, from impacting physical performance to causing severe medical conditions, such as heart failure exacerbated by diuretics or improper blood circulation.
Despite the critical nature of maintaining appropriate hydration levels, there's a significant gap in prompt, real-time monitoring solutions. Existing methods, often reliant on blood tests or external body symptoms, are cumbersome and lack immediacy. This void becomes especially crucial considering populations at higher risks of dehydration, such as athletes, military personnel in extreme environments, hospital patients, infants, the elderly, and even individuals who fast for religious or cultural reasons(2). Given these complexities, there's a growing need for non-invasive, real-time hydration monitoring systems.

Recent developments in wearable technology offer a promising avenue for addressing these challenges(3). These wearables, ranging from smartwatches to smart clothing, can monitor hydration by measuring the electrolyte changes in sweat or assessing hydration at a cellular level through electrical or optical sensors. Advances in near-infrared spectroscopy (NIRS) provide additional avenues for hydration assessment based on the optical properties of tissues. These technological strides have been pivotal in providing a continuous, non-invasive means to gauge hydration status, thereby having the potential to mitigate risks and improve the quality of life for various at-risk populations.

This section aims to provide a brief review of recent advances in wearable devices employing electrical and optical methods for non-invasive hydration monitoring. To provide context, we consider several populations at a greater-than-average risk for developing dehydration: athletes, military personnel in harsh environmental settings, individuals involved in infant and maternal health, and the elderly. Specifically, we will delve into the medical and operational causes and consequences of dehydration among these populations, informed by advancements in wireless body sensor networks for health-monitoring applications (4). Moreover, we will discuss existing and emerging methods and their capabilities, focusing on those that offer real-time monitoring advantages.

1.1 Health Monitoring Across Different Populations: Innovations in Wearable Biosensors

Here, we offer a sneak peek into the advancements in wearable biosensors designed for monitoring various demographics and discuss the essential considerations involved.

Elderly Health Monitoring: Continuous health trackers requiring minimal intervention are highly desirable for the elderly. This is because Many older persons (i.e., those 65 years of age and older) with chronic diseases and/or functional impairment are in a state of mild hyper tonic dehydration due to a variety of factors. Wearables like smartwatches, smart clothing stand out due to their potential to incorporate a variety of sensors. These garments have applications in cardiac monitoring, chronic obstructive pulmonary disease management, and hydration monitoring. Specifically, Sweat-based wearables, such as colorimetric and electrochemical biosensors, allow for non-invasive sampling. Electrochemical biosensors, in particular, provide

continuous electrical readouts, making them valuable for real-time health status monitoring in the elderly.

Infant and Maternal Health Monitoring: For neonates and infants, adaptations of adult-designed sweat-based electrochemical biosensors can be useful. Monitoring multiple biomarkers—such as temperature, hydration, and pulse rate—is essential in neonatal intensive care units and at home. Devices that are low-cost, low-maintenance, and have long battery life are crucial. Electrochemical biosensors are attractive for these applications due to their microfabrication compatibility and real-time monitoring capabilities.

Military and Harsh Environmental Settings: In military contexts, wearable sensors are critical for monitoring personnel in extreme conditions. Risks such as dehydration, altitude sickness, and electrolyte imbalances can affect soldiers' performance and health. Real-time hydration tracking via wearable patches can offer essential data for timely interventions. Electrochemical biosensors are especially suited for this, but challenges like power supply, data transmission, and durability remain.

1.2 Literature Review

To compile relevant research papers information, an extensive literature search was conducted. The search aimed to identify recent advancements in hydration monitoring wearable technologies. Reviews on the topic(5) usually classify hydration system based on the type of sensors used for hydration monitoring wearable technologies. By studying the number of papers (Figure 1) we notice the two most prevalent categories are Electrical-based and Optical-based. Electrical-based hydration tracking methods appear to dominate the current research landscape. This could be attributed to the well-established relationship between electrical properties of skin and hydration levels. Optical-based solutions, While fewer in number compared to electrical methods, offer unique advantages, such as the ability to gather detailed molecular information about skin hydration. These methods are particularly well-suited for applications requiring precision, such as medical diagnostics. The relatively higher complexity and cost associated with optical sensors may explain the smaller number of publications, but their potential impact on healthcare and research is significant.

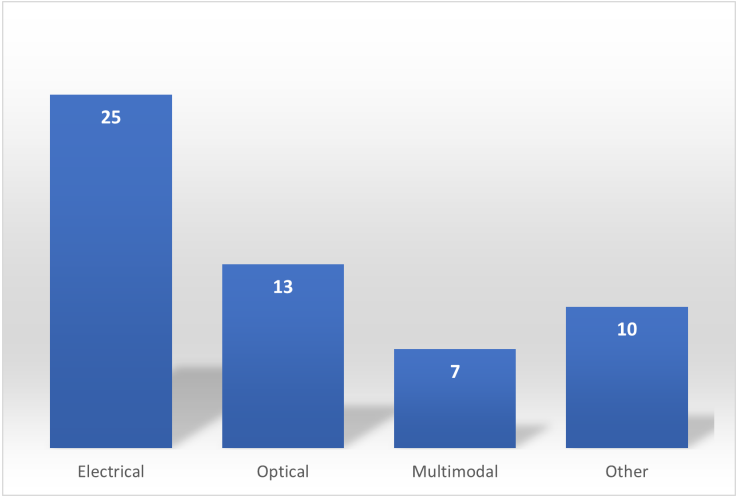

Figure 1: Number of publications of Hydration monitoring system categorized based on the type of sensors used.

1.2.1 Optical Sensors

Typically, noninvasive this method involve shining light at a specific wavelength onto the skin to collect data. A sensor then detects the light that is reflected, absorbed, or refracted. The wavelength of light is crucial for determining how deeply it penetrates the skin when transmitting an optical signal, and that's what mainly differentiate between the different techniques including Raman spectroscopy, near-infrared spectroscopy and other Light based spectroscopes. Table 1 depicts different Biomarkers, the Wavelength Range at which they are detected, and Authors of the research. These techniques offer valuable insights into skin hydration levels, with applications spanning from sports performance optimization to infant and maternal health monitoring. However, their widespread adoption may require addressing challenges related to sensor miniaturization and cost-effectiveness.

Biomarkers	Wavelength Range	Authors
Temporal changes in reflected speckles	green laser (532 nm)	Y. Tzabari et al.(6)
Minute variations in wrist hydration	microwave range (2-6 GHz)	I. Butterworth et al.(7)
UV exposure	IR spectroscopy	R. Benavides et al.(8)
pH levels in sweat	smLED at visible light (300-700nm)	F. Curto et al.(9)
multiple dermal health markers	(UV)-sensitive photodetector	O. Polat et al.(10)
Temporal changes in reflected speckles	600 to 1150 nm	N. Ozana et al.(11)
Diffuse reflectance spectroscopy to detect fluid status	530 to 950nm	V. Sandys et al.(12)
Water, Proteins, Lipids, and other skin constituents	750–2500 nm	M. Mamouei et al.(13)
Water absorption peaks	940, 970, 1200, and 1450 nm	M. Mamouei et al.(14)
Peak values around water overtone and combination bands	900-2100 nm	M. Qassem et al.(15)
Temperature and Water content	750–2500 nm	A. Bohman et al.(16)
Localized percentage water content (PWC)	650-900 nm	R. Van Beers et al.(17)
Skin water content	1300-2000 nm	H. Arimoto et al.(18)

Table 1: Table of Biomarkers, Wavelength Range, and Authors

1.2.2 Electrical Sensors

Electrical-based biosensors range from Capacitance and conductance-based to impedance-based systems, they emerged as a noteworthy approach to to provide real-time data on hydration status. Their ability to measure electrical properties of the skin, influenced by water content, provides valuable quantitative data. Their non-invasive nature and ability to integrate seamlessly into wearable devices make them a valuable tool for continuous monitoring. Despite these advantages, they have limitations in assessing deeper skin layers, and their performance might be influenced by factors such as ambient conditions and skin temperature. Note that Multi-Modal Sensors represent papers that investigate wearable devices combining multiple sensor modalities to enhance hydration monitoring accuracy and reliability. Other Sensors are based on other type of sensors, such as Electromagnetic, thermal, and others...

1.2.3 Commercial Hydration monitoring products

In addition to academic research papers, a comprehensive analysis of commercial products within the field of hydration monitoring was conducted. Various companies actively involved in developing and marketing hydration tracking wearables were identified through thorough online research. Detailed assessments were performed to compare the technological features, functionalities, and applications of these commercial products. This analysis provides valuable insights into the practical implementations and advancements in the field, bridging the gap between academic research and real-world applications.

Category	Product name	Features	Validated	Commercially available	Company	Technology
Wristband	BioPtx(19)	Hydration, Temperature, HR, HR variability, Respiratory rate, Blood saturation	No	No	Rockley	IR laser tech (36 wavelengths),PPG: green, red, infrared, Accelerometer
Wristband	Sixty(20)	Hydration, HR, activity levels, calories burnt, sleep tracking	No	No	Sixty	optical spectrometry. Three LEDs shine green, red and infrared light.
wristband	LVL(21)	Hydration, tracking activity, sleep, mood and HR, calories.	No	No	BSX Athelet-ics	Red light technology.
Wearable band	hDrop Gen2 (22)	Hydration and Body temperature.	No	Pre-Order	hDroptech	Electrode tracks sweat loss and rate, sweat, sodium, and potassium levels.
Smartwatch	Geca sensor(23)	Hydration.	Yes	Pre-Order	hydrostasis	Optical spectroscopy, detect fluid concentration in the skin.
Smartwatch	Aura Strap(24)	HR, blood saturation, hydration.	No	No	Apple	Electrode measure electrolytes in sweat to monitor hydration .
Smartpatch	Gx Patch(25)	Hdyration, sweat, electrolyte content, body temperature	Yes	Yes	epicore Biosystems	a thin microfluidic substrate on the skin that captures sweat .
Smartpatch	Hydration Biosensor(26)	Hdyration	Yes	Yes	Nix	Electrodes detects electrochemical biomarkers in sweat.

Table 2: Overview of Wearable Hydration monitoring system products

Table 2 presents a comprehensive overview of various hydration monitoring products, each offering unique features and technologies. Notably, some products, like Rockley's BioPtx, employ advanced IR laser technology and multi-sensor capabilities for monitoring various health parameters, although they are yet to be validated and made commercially available. On the other hand, products like the Nix Hydration Biosensor and Gx Patch have undergone validation and are readily available for use. These diverse offerings cater to different user preferences and requirements, highlighting the evolving landscape of hydration monitoring technologies. As we explore each product in detail, we'll gain valuable insights into their potential applications and benefits in real-world scenarios.

1.2.4 Difference between Wearables and Clinical Lab methods for hydration tracking

Wearables offer convenient and cost-effective options for hydration monitoring, making them accessible to a wide audience and enabling the identification of baseline trends. However, concerns about their reliability, lower clinical accuracy, limited fluid analysis capabilities, and susceptibility to confounding factors are notable shortcomings. On the other hand, lab and clinical methods provide high validity and trustworthiness, having gained regulatory approval, but they are primarily suitable for clinical use due to their cost, instrument and personnel requirements, and the need for combined analyses. They also face challenges related to confounding factors. The choice between wearables and lab/clinical methods depends on specific needs, ac- curacy requirements, and practicality for the intended application. In the current market, optical-based wearables dominate, possibly due to their cost-effectiveness.

1.3 Contributions

- Our objective was to create a non-invasive monitoring system capable of assessing hydration levels, even in the absence of sweat, by analyzing electrolyte levels in the bloodstream.
- We seamlessly incorporated an affordable spectrophotometer into an open-source smartwatch.
- The prototype provides on-device data analytics and evaluation, eliminating the need for Wi-Fi or cloud computing.
- Our study presents a distinctive contribution by exploring the correlation between emotions and light absorbance, representing a novel endeavor in connecting emotional states with physiological data.

2 Methods and Implementation

When we drink water, water molecules are absorbed in intestinal track and are distributed through blood through the whole body. Using an optical sensor that can send light through the skin, we can measure the fluid concentration. Different wavelength of lights are sensitive to different molecules in the tissue. In our solution we use a sensor that measure photons scattered back to the detector(27). The goal is to design an algorithm that defines an optimal hydration range through the 'personal hydration index', providing notifications when we are below or above the optimal range. We integrated a multi wavelength spectroscopy sensor that combines the precision of clinical spectroscopy setups, with the portability and low-cost of LEDs into a wearable watch.

2.1 Hardware and Experimental setup

2.1.1 SparkFun Triad Spectroscopy Sensor-AS7265x

The SparkFun Triad Spectroscopy Sensor(28) is a low-cost spectrophotometer based on three AS7265x spectral sensors connected to a visible, UV, and IR LEDs to illuminate and measure absorbance (photon scatter) of different surfaces. The Triad combines 3 Integrated circuits (ICs) AS72651, the AS72652, and the AS72653 and can detect lights from 410nm (UV) to 940nm (IR). 18 individual light frequencies can be measured with precision down to 28.6 nW/cm2 and accuracy of +/-12%, making previously unaffordable equipment accessible on a regular desktop or portable setup. Figure 3 shows how each of the three ICs is connected to

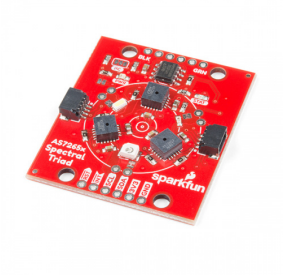

Figure 2: SparkFun Triad Spectroscopy Sensor

a specific LED, and how the whole setup offers communication over I2C. An Arduino library is used to access all the various features include taking readings and illuminating LEDs over the I2C interface.

2.1.2 Measuring absorbance with the Triad Spectroscopy Sensor

The sensor array permits us to measure and characterize how different materials absorb and reflect 18 different frequencies of light. The x-axis represents the wavelength and y-axis represents the raw absorbance response. For example to differentiate between elements, we can measure their raw absorbance by plugging the sensor to an Arduino MCU and take a baseline reading for each sample. Now that we have a baseline we can take a reading from an unknown thing and after comparing the new graph we can see that the unknown sample is in fact Uranium (Figure 4).

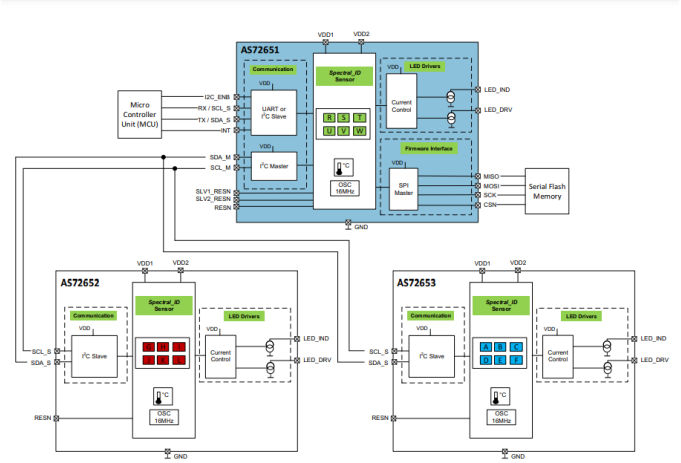

Figure 3: AS7265x Chip-Set Block Diagram

2.1.3 Hach DR3900 Laboratory Spectrophotometer

To evaluate the precision of the low-resolution Triad spectroscopy sensor, we employ the Hach DR3900 Laboratory Spectrophotometer(29). This benchtop spectrophotometer operates within the visible spectrum (320 - 1100 nm) and offers more than 220 pre-configured methods tailored for laboratory water analysis. Keeping water analysis tasks in focus, the DR3900 spectrophotometer is specifically engineered for both safety and precision.

2.2 Use case 1: Electrolyte solution spectroscopy

In this study, we want to calibrate and benchmark our sensor with the Hach DR3900 Laboratory Spectrophotometer, in the following subsections, we will perform experiments where we measure the absorbance of different solutions with the triad sensor and compare them to the DR3900.
Absorbance, which is used in spectrophotometry, relates to the amount of light absorbed by a material. The equation for absorbance (A) is given by A = log10(I0 / I), where I0 is the intensity of the incident light and I is the intensity of the transmitted light. The AS7265x sensor provides the raw intensity of light at various wavelengths, while the Hach DR 3900 outputs absorbance values, essentially taking the logarithm of the ratio of incident to transmitted light intensity for you. To convert the analog output from the AS7265x sensor to absorbance values, we follow these steps:

Calibrate the sensor: Before we start making measurements, we need to calibrate the sensor. We do this by using a known light source with a known intensity (I0).

Measure the incident light (I0): We measure the intensity of the incident light (I0). We do this by positioning the sensor so that it receives the light directly from the light source without any sample in the way.

Measure the transmitted light (I): Next, we measure the intensity of the transmitted light (I). We do this by placing the sample between the light source and the sensor, and then taking a measurement.

Calculate the absorbance (A): After we have these two measurements, we can calculate the absorbance (A) using the formula A = log10(I0 / I).
This process will give us the absorbance at the specific wavelengths your AS7265x sensor

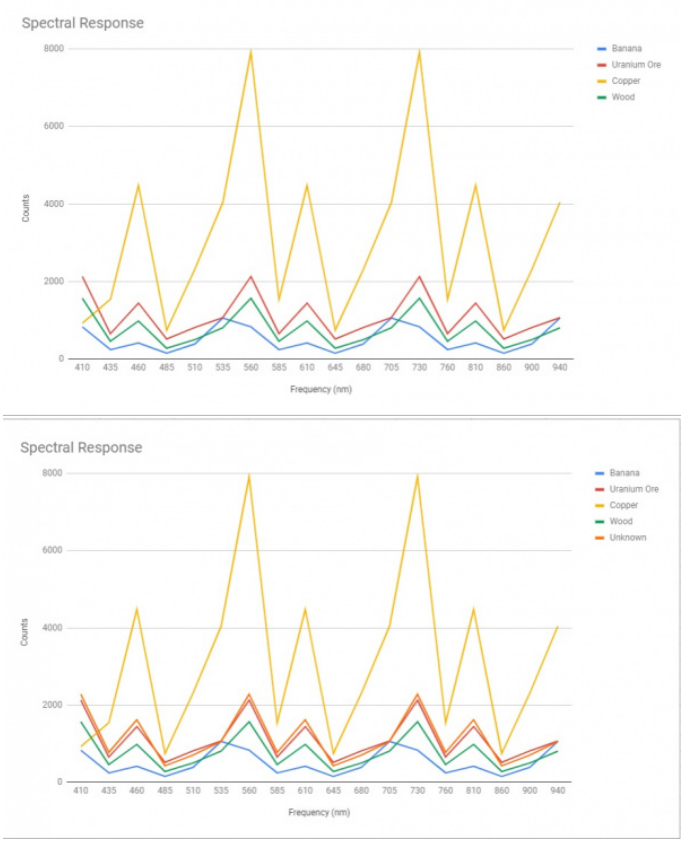

Figure 4: Comparing Unknown sample to the baseline reading

is capable of measuring, allowing to compare the readings with the output of the Hach DR 3900. Measuring the incident light (I0) is critical to calculate the absorbance in the setup. Unfortunately, with the AS7265x sensor, there's no direct way to measure the incident light (I0) using the Arduino library because the sensor is not designed to make these measurements. A common practice in spectroscopy to get around this limitation is to measure a reference or blank sample, usually a solution or material that does not absorb light in the wavelengths of interest. This blank sample measurement serves as an estimate of the incident light (I0). Here are the steps to do it:

Choose a blank sample: This sample should not absorb light in the wavelengths of interest. It could be a solution known not to absorb at those wavelengths or simply the solvent if you're doing solution measurements. Measure the blank sample: Position the blank sample between the light source and the sensor, and measure the intensity using the getCalibratedX() function where X is each of the 18 channels available. Making sure to let the sensor warm up and gather several readings over time to ensure a stable and accurate measurement. Store the values: The readings from the blank sample serve as our I0 value for each of the wavelengths. We store these values so they can be used later for calculating absorbance.

2.2.1 Calibration with sodium-based Solution

To ensure accurate calibration of our sensor using the DR3900 Laboratory Spectrophotometer, we opted for a liquid sample that would exhibit a distinct peak, facilitating a more straightforward comparison. In pursuit of this objective, we conducted an analysis on POWERADE® MOUNTAIN BERRY BLAST, a beverage renowned for its claim of containing 50%

Figure 5: Hach DR3900 Laboratory Spectrophotometer

more electrolytes than the leading sports drink. Additionally, each bottle of POWERADE® MOUNTAIN BERRY BLAST boasts a substantial 240mg of Sodium, a crucial parameter for assessing hydration levels in blood.
Subsequently, the measurement of absorbance for the POWERADE® sample with the DR3900 yielded the outcome shown in figure 6.

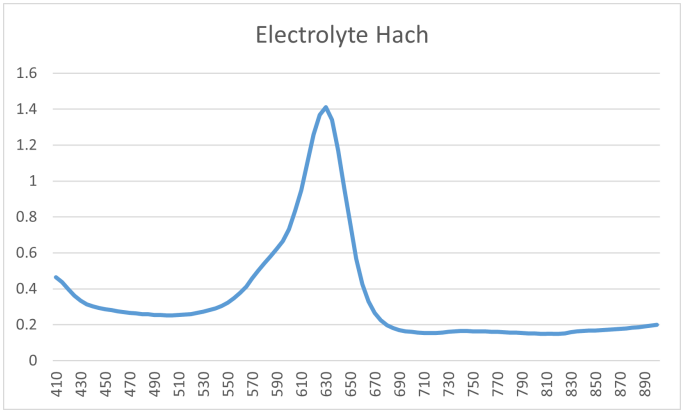

Figure 6: Measuring the absorbance of the PowerADE sports drink with the DR300

Note that the graph shows a significant peak around the 630nm wavelength, which correspond to the sodium detection peak found in the literature.
After calibrating the gain of some of the channels of the Triad sensor, we analysed the same sample and obtained the graph shown in figure 7.

We observed a peak similar to the one we obtained from the DR3900 spectrometer, and thus this experiment showed us that despite the low resolution, the Triad can be reliable to further investigate other hydration biomarkers.

2.2.2 Sodium-Chloride solution at different concentrations

On the next experiment, we wanted to perform the same comparative analyses by measuring sodium-chloride absorbance through different concentration. Chloride electrolyte is another key element to evaluate hydration, thus we wanted to experiment through different concentration to see if we can actually see the difference in concentration through our absorbance analyses. The graphs in Figure 8 is the results obtained by measuring the absorbance of a 200mg then 400mg sodium-chloride solution.
As expected, the solution with higher concentration gives higher absorbance, with a relatively

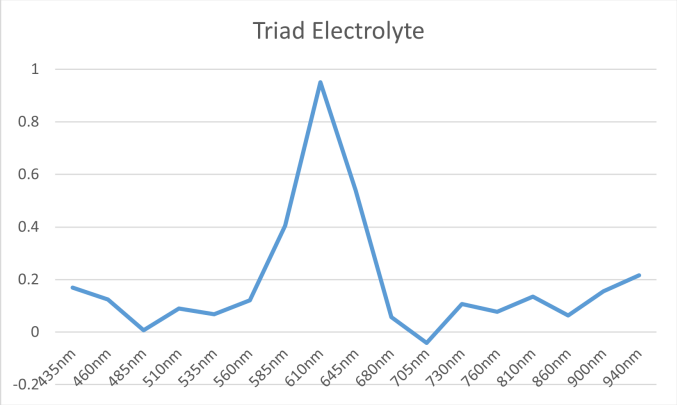

Figure 7: Measuring the absorbance of the PowerADE sports drink with Triad spectroscopy sensor

close absorbance between the results obtained using the Triad spectroscopy sensor and the DR3900.

2.2.3 Potasium-Chloride solution at different concentrations

Next we wanted to investigate the absorbance of a potassium chloride solution at different concentrations. We started at a higher concentration (600mg dilluted in 10ml of water), and compared the results of the triad sensor and the DR3900 across 4 concentrations. We obtained the results shown in Figure 9.
In both sets of data, there is a general trend where the absorbance values increase with increasing potassium chloride concentration. This relationship is expected in spectrophotometry, where absorbance is directly proportional to the concentration of the analyte.
Again the results shows that teh abosrbance measured by the triad sensor is relqtively close to the one we are getting with DR3900 which encourages us to pursue our experiment on hydration level. Overall, this experiment provides valuable data for understanding how the Triad sensor performs in measuring absorbance compared to a well-established spectrophotometer like the DR3900.

2.3 Device Integration

2.3.1 DSTIKE Deauther Watch V4

The DSTIKE WATCH V4(30), is an open-source smartwatch equipped with the ESP32 micro-controller, serves as an optimal platform for deploying TinyML models on the edge due to its favorable memory characteristics. The ESP32 micro-controller, part of the Espressif Systems family, is renowned for its efficiency and versatility, making it a popular choice for edge computing applications. In the context of deploying machine learning models, memory constraints play a crucial role, and the ESP32 addresses these concerns adeptly.

The ESP32 micro-controller within the DSTIKE WATCH V4 boasts a dual-core processor and is designed with consideration for low power consumption. For machine learning applications, particularly those involving TinyML models, where memory efficiency is paramount, the ESP32's flash and RAM specifications make it well-suited for deployment on resource-constrained devices. The ESP32 typically provides a sufficient amount of flash memory for storing the model parameters and code, while its RAM capacity allows for efficient execution of inference tasks.

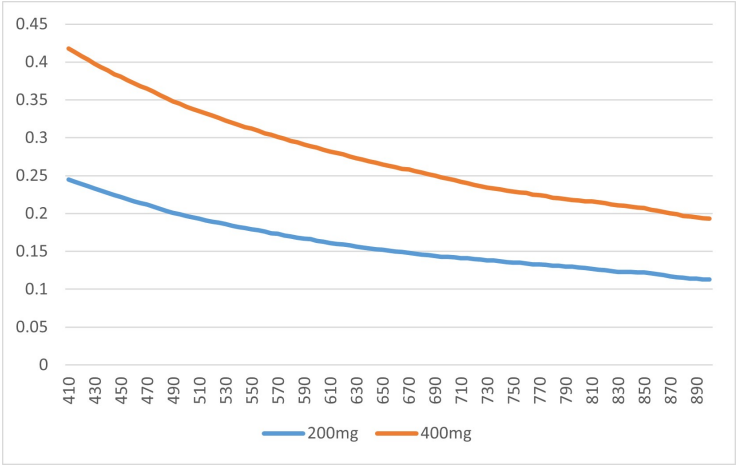

((a)) DR3900 Spectrometer Results

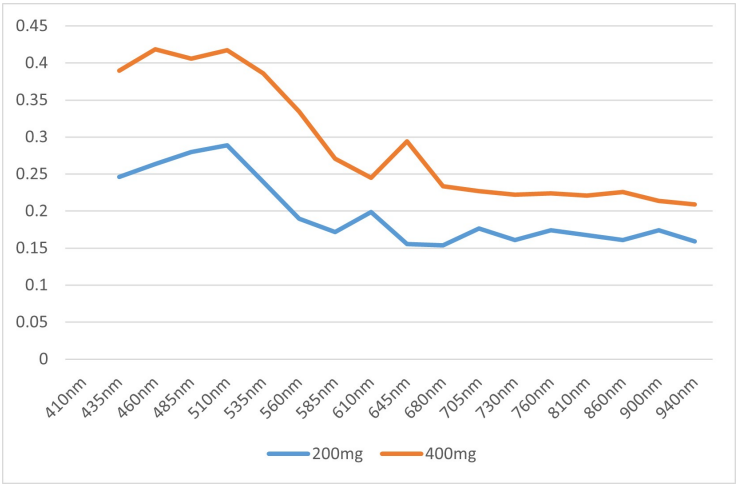

((b)) Triad Spectroscopy Results

Figure 8: Sodium-Chloride solution absorbance at different concentrations

In the context of the DSTIKE WATCH V4, which integrates the ESP32, the device strikes a balance between compact design and computational capability. The inherent memory efficiency of the ESP32 aligns with the DSTIKE WATCH V4's form factor and power constraints, making it an ideal candidate for deploying AI models directly on the wearable device. This combination of compact design, low power consumption, and ample memory resources positions the DSTIKE WATCH V4 as a reliable platform for real-time, edge-based AI applications, including the execution of TinyML models.

2.3.2 Prototype of the Smartwatch

The figure below shows how we integrated the triad spectroscopy sensor to the DSTike watch, with the lights facing the bottom of the watch to target the wrist. We soldered the I2C pins of the sensors to the open I2C pins of the dstike watch, and used a plastic case to encapsulate the whole system.
Note that we program we are using the Arduino software to program the watch and interface to the Triad spectroscopy sensor, we also have a USB interface to visualise and debug data real-time via the DStike serial port.

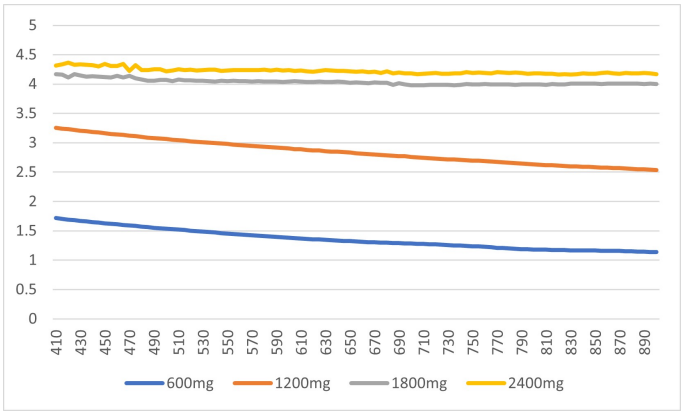

((a)) DR3900 Spectrometer Results

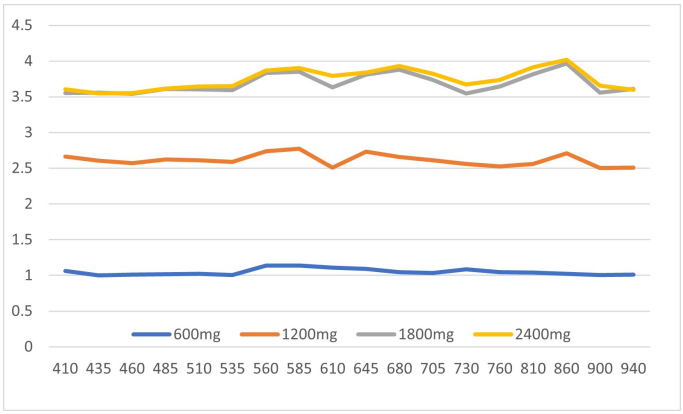

((b)) Triad Spectroscopy Results

Figure 9: Potassium-Chloride solution absorbance at different concentrations

2.4 Use case 2: Skin hydration monitoring

In this specific scenario, our objective is to assess hydration levels by analyzing spectral data obtained from the skin. To achieve this, we conducted a series of experiments involving participants. These experiments included data collection at multiple time points: initially when the participants were well-hydrated before commencing a workout session, then during the middle of the workout, and finally, at the workout's conclusion, with no water intake allowed throughout the entire workout duration. Additionally, we also conducted measurements in the early morning when individuals typically experience dehydration before consuming fluids, and later the day when the participants are fully hydrated. Our study cohort was constituted of 5 participants, 6 males aged between 20 and 32.

2.4.1 Data Collection

a. Morning Measurement (Presumed Dehydration upon Waking):
Timing: Asking participants to take the first measurement immediately upon waking up, before consuming any fluids.
Environment: Making sure the room is sufficiently lit and free from significant temperature changes.
Duration: 6 minutes of continuous measurements. (Keeping 5 minutes after cleaning noise).

Figure 10: DSTIKE Deauther Watch V4

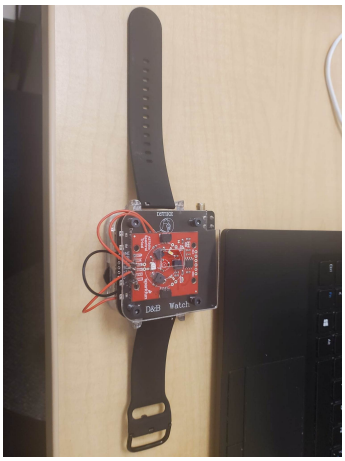

Figure 11: Integration of the Triad Spectroscopy sensor to the DStike Watch

b. Pre-workout Measurement (Fully Hydrated):
Hydration: Asking participants to drink a specified amount of water (e.g., 500ml) 30 minutes before the workout. This ensures hydration without them feeling too full during the workout.
Environment: The same environment as the workout to minimize external variability.
Duration: 5 minutes of continuous measurements. (Keeping 5 minutes after cleaning noise).

c. Mid-workout and Post-workout Measurements (Progressive Dehydration):
Depending on the workout's intensity and type, this could be halfway through the session.

d. Post-workout: Immediately after the workout ends.
Since we are trying to classify hydration status using spectral data from skin, determining a consistent (reference light intensity) is vital. We do that by measuring the Ambient Light:
We do this by bringing a sensor placed nearby, not in contact with the skin. This sensor would be continuously measuring the incident light without any interference from the skin. This method has the advantage of continuously providing a measure of the ambient light conditions, which could change due to factors like the light source aging or external light interference.

2.5 Machine Learning, 3 hydration status classes

In this section we dive into the machine learning analyses. We tried two different approach, we first considered the data of all participants to train a model and classify the 3 classes of: fully-

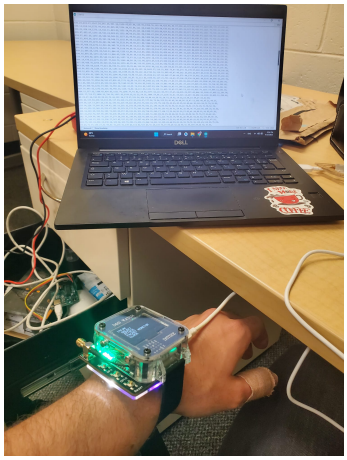

Figure 12: Fasting experiment setup

hydrated, mid-hydrated and dehydrated. On the second approach we isolate every participant data during the training and generate a model specific to the individual. We want to conduct initial aggregated analyses to identify common patterns and then delve into individual-level analyses to account for variations and specific insights.

2.5.1 Aggregate Analyses

The goal here is to analyze and model the hydration states on an aggregated level, combining data from all participants into a single CSV file allowing to have a larger dataset for modeling, which can potentially lead to more robust and generalizable results.

2.5.2 Analyzing Each Participant Individually

Studying individual variations in hydration states may give us insight on how hydration affects each participant differently, analyzing each participant's data separately may be more appropriate.

2.5.3 Correlation Analyses

To study the similarities in the data we gathered, we generated a cross-correlation matrix where rows and columns of the matrix correspond to the sensor channels and every channel represent a specific wavelength. The values in the matrix represent the degree of similarity or correlation between pairs of sensor channels. Strong positive or negative values off the diagonal for specific pairs of sensor channels, suggests that these channels tend to behave similarly or in an opposite manner with a specific time lag. In signal processing, cross-correlation can be used for tasks like time-delay estimation or pattern recognition. When analyzing the whole matrix, we will be looking for overall patterns and relationships. Are there clusters of sensor channels that show similar behavior. Interpreting the cross-correlation matrix can provide insights into how different sensor channels interact and whether certain patterns or relationships are present in the data.

2.5.4 Feature Extraction

In our study, the absorbance data obtained during the experiment exhibited a narrow range of variation. Recognizing the need to extract meaningful features from this limited variability,

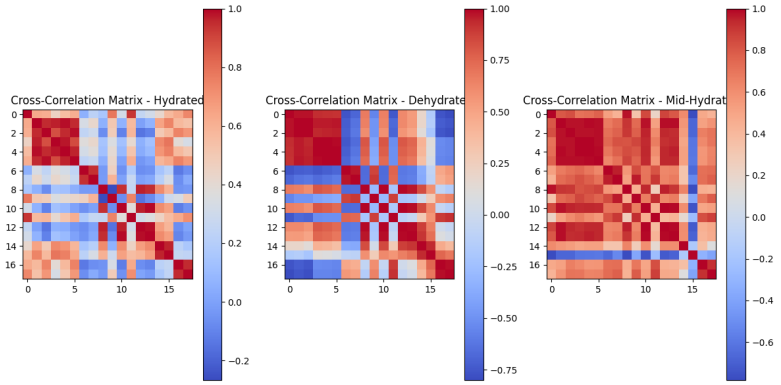

Figure 13: Aggregate cross-correlation Matrix

we employed Eulerian Video Magnification. Unlike traditional methods, Eulerian Video Magnification acts as a sophisticated amplification technique, enhancing subtle changes within the data. This is particularly crucial in our context, as these amplified variations may signify significant physiological events or anomalies that might not be readily apparent in the raw, unprocessed data. By utilizing Eulerian Video Magnification, we aimed to uncover nuanced patterns and fluctuations that could serve as valuable indicators of underlying physiological dynamics related to hydration status. This approach allows for a more detailed and insightful analysis, helping to capture and highlight subtle changes that might hold key information for our investigation(31). We also use a Butter-worth band-pass filter reducing noise, and enhancing the components of interest. Figure 14 shows the difference between the original signal and the Euler-Magnified Signal, we notice that the transform permits us to generate extended changes from signal variations. The signal obtained from the Euler Video Magnification can

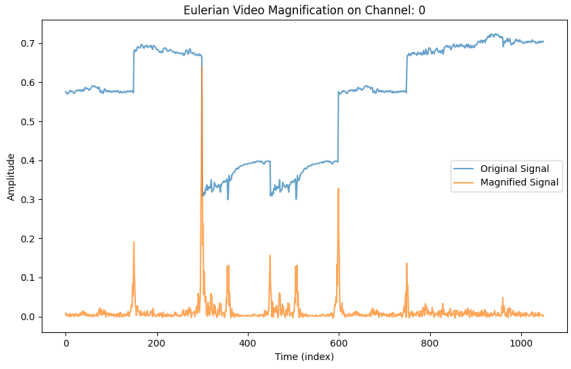

Figure 14: Input vs Magnified Signal

serve as features for our hydration classifier and can be used to describe the characteristics of the data. These features will be fed into machine learning models to build a classification model. Figure 15 shows the overall pipleline of our data pre-processing.

2.5.5 Multimodal Analyses

We conducted experiments with three distinct models for our hydration status classifier. The initial model was a Support Vector Machine (SVM) classifier utilizing a linear kernel and a regularization parameter (C) set to 1.0. The second model was a Random Forest classifier

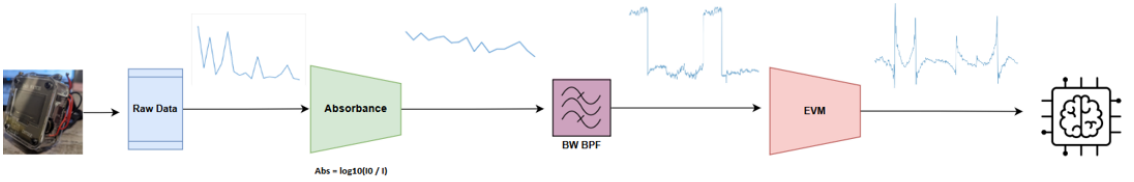

Figure 15: Machine Learning Model PreProcessing Pipeline

with 80 estimators and a random state of 42. After observing that the Random Forest model exhibited superior performance compared to the SVM model, we also implemented the XGBoost model. Further details on the outcomes of these experiments will be elaborated upon in subsequent sections.

2.6 Implementing the AI algorithm on the Edge

The traditional workflow of cloud computing has noted several drawbacks with the continuous growth of IoT application. Centralizing all the processing in the cloud not only keeps raising latency and bandwidth issues, but it also creates a major vulnerability in terms of privacy and security. The next step in IoT will be to deploy AI models on the edge as an alternative to going through the cloud. The new process involves training on the cloud or on powerful machines (supercomputers for example), save the best parameters, and run them on the edge. In fact this method is useful for applications like critical analysis and patient monitoring since it reduces needless processing time and data traffic(32).
It is now simpler for developers to create apps for these devices thanks to improved hardware and more effective development standards, the most popular trend being TinyML, a compact version of Machine Learn- ing permits the inference of ML models and to run complex deep learning models on microcontroller-based embedded devices that are also cheap, and require less resource and power consumption(33). Tensor Flow Lite Micro (TF Lite Micro) is the most used TinyML framework, it is python based and was specifically designed to get integrated into micro-controller units (MCUs)(34). It is used to deploy ml on mobile device and embedded systems, the interpreter currently supports a limited subset of TensorFlow operators that have been optimized for on device use. This means that some models require additional steps to work with TensorFlow Lite. We don't have to either master Machine Learning nor C++ to successfully train, convert and deploy a TinyML model to an Arduino board for example, starting from scratch. It usually takes a line of code to convert the machine learning model (h5) into it's embedded version (header file).

2.6.1 Deploying our ML model in the Watch

To run a TinyML model, we will make use of Python and the everywhereml package, which is a wrapper around the well-known scikit-learn package. We will go with the Random Forest Classifier we trained on the data described earlier, because it's fast and accurate. As mentioned previously, the package permits us to convert the model to a header file in a couple lines of code. To deploy the model into our system, we import the header to the Arduino software, and modify the code accordingly.
We choose to implement the Random Forest algorithm because, Generally, Random Forests are less memory-intensive compared to boosting algorithms like XGBoost. Random Forests consist of multiple decision trees, each of which is simpler and requires less memory. The ensemble of decision trees in a Random Forest is usually smaller in size compared to the

ensemble in XGBoost. This is because Random Forests don't require the intricate boosting logic present in algorithms like XGBoost. Considering these factors, and our primary concern being simplicity, memory usage, and ease of implementation on resource-constrained devices like the DSTIKE watch MCU, Random Forest feels like a more suitable choice.
A Random Forest Classifier can execute in 10 microseconds on an input of 1000 features and it requires less then 1 Kb of RAM.
The final prototype average the absorbance collected over a minute period, runs the model and display the hydration on the OLED screen. We also used the LED in the Watch to indicate the hydration status as follow: Green for fully hydrated, blinking green for mid-hydrated, and Red for dehydrated. The diagram below summarizes the described workflow:

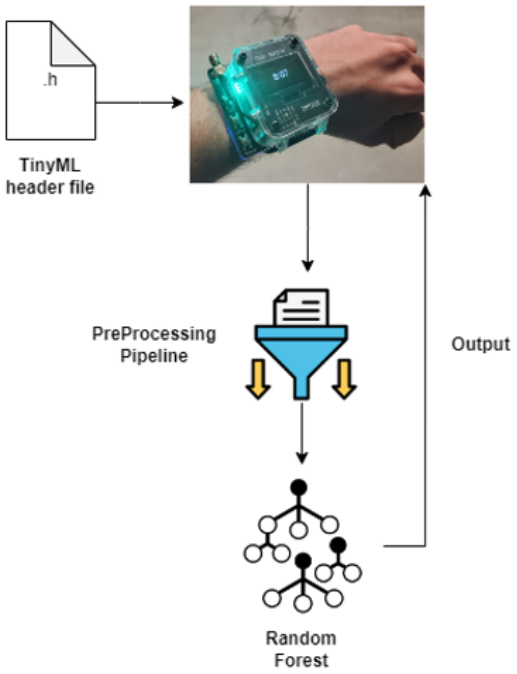

Figure 16: Deploying our Hydration Status model on the edge

3 Results

3.1 Aggregate Analyses

In the aggregate analyses, the examination of raw signal statistics yielded limited insights. However, more sophisticated techniques, such as cross-correlation matrices and wavelet transform heatmaps, provided a richer understanding of the data. Notably, distinct patterns emerged, offering a nuanced representation of hydration states.

The performance of three classifiers was rigorously evaluated. The Random Forest classifier exhibited a commendable accuracy of approximately 84%, demonstrating its proficiency in hydration classification. Surpassing this, the XGBoost classifier achieved an impressive accuracy of around 95%, showcasing its superior predictive capabilities. Specific class-wise results in precision, recall, and F1-score were tabulated for both classifiers, emphasizing their efficacy across different hydration states.

Table 3: Random Forest Classifier Results

Class	Precision	Recall	F1-Score
Fully Hydrated	0.70	0.94	0.80
Mid-Hydrated	0.92	0.80	0.85
Dehydrated	0.96	0.78	0.86

Table 4: XGBoost Classifier Results

Class	Precision	Recall	F1-Score
Dehydrated	0.96	0.95	0.95
Fully Hydrated	0.93	0.96	0.94
Mid-Hydrated	0.96	0.95	0.95

Cross-validation of the Random Forest classifier demonstrated consistent accuracy across 5 folds, with a mean accuracy of 83% and a minimal standard deviation of 2%. ROC curve analysis further validated the models' ability to discriminate between hydration states, with ROC (Receiver Operating Characteristic) AUC (Area Under the Curve) values providing quantitative insights. We also plotted the training and validation score of our Random forest classifier, to evaluate the overfiiting. The observed results from the training and validation scores across the 5-fold cross-validation of our Random Forest classifier provide insights into the model's performance and potential overfitting. The average training score of 85.7% indicates that the classifier has learned well from the training data, achieving a high level of accuracy during the training phase. The assessment of overfitting through the training and validation scores revealed a well-learned Random Forest classifier, with an average validationscore of 82.7%. The low difference between training and validation scores indicated good generalization, suggesting resilience against overfitting.

3.2 Analyzing Each Participant Individually

Individual participant analyses unveiled intriguing patterns in model performance. The Random Forest classifier displayed variability among patients, with Patients 3,4 and 6 achieving higher accuracy. Patient 5 presented challenges, indicating potential influences of individual

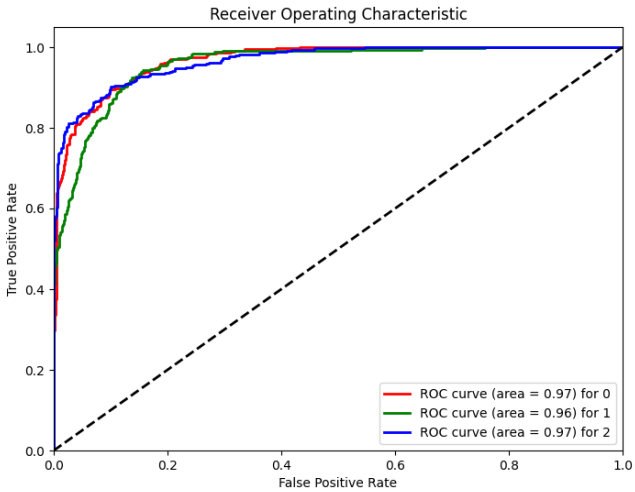

Figure 17: ROC curve for the three hydration classes

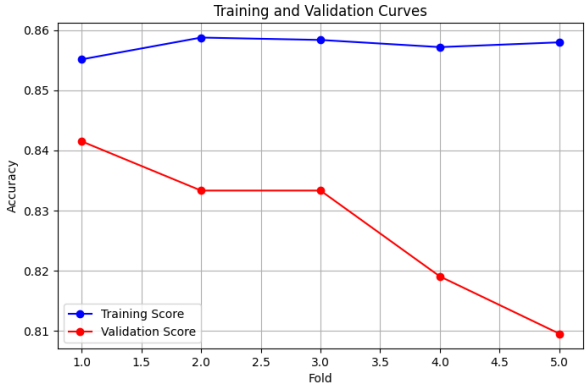

Figure 18: Training score vs Validation score accross 5 folds

characteristics on model efficacy. In contrast, the XGBoost classifier consistently outperformed the Random Forest model across all patients, with Patient 4 standing out with the highest accuracy. The nuances in accuracy underscored the need for a nuanced understanding of individual responses to classification models. Overall, these accuracy results suggest that both the Random Forest and XGBoost models perform well across individual participants, with XGBoost generally demonstrating slightly higher accuracies. The variability in accuracy across participants may be influenced by individual characteristics or data quality.

The graphical representations, including ROC curves and training vs. validation scores, provided visual insights into model discrimination ability and generalization. These results collectively emphasize the success of machine learning in hydration monitoring while acknowledging the importance of considering individual variations for personalized model applications.

((a)) Random Forest Classifier Accuracy

Participant	Accuracy	mean validation	validation std
Participant 1	0.85	0.88	0.03
Participant 2	0.83	0.84	0.02
Participant 3	0.87	0.86	0.02
Participant 4	0.93	0.91	0.02
Participant 5	0.74	0.85	0.06
Participant 6	0.87	0.82	0.04

((b)) XGBoost Accuracy

Participant	Accuracy
Participant 1	0.94
Participant 2	0.89
Participant 3	0.91
Participant 4	0.95
Participant 5	0.86
Participant 6	0.89

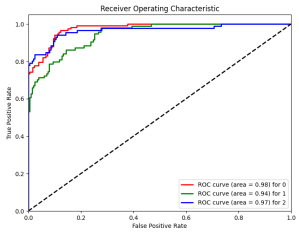

((a)) Participant 1 ROC curve

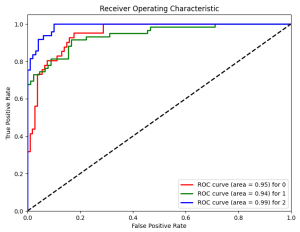

((b)) Participant 2 ROC curve

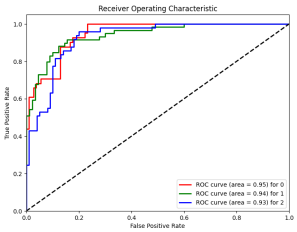

((c)) Participant 3 ROC curve

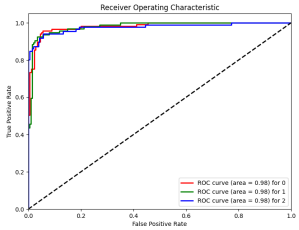

((d)) Participant 4 ROC curve

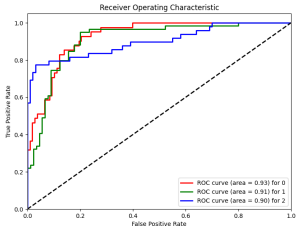

((e)) Participant 5 ROC curve

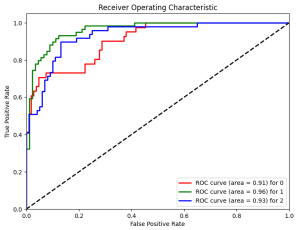

((f)) Participant 6 ROC curve

Figure 20: Individual ROC curves of the six participants

4 Discussions

In the aggregate analyses, the exploration of cross-correlation matrices and wavelet transform heatmaps revealed nuanced variations among the three hydration states. Despite limited insights from raw signal statistical analyses, the distinctive patterns extracted through cross-correlation and wavelet transforms highlight the potential for advanced signal processing techniques in discerning hydration status. Moving beyond signal exploration, the application of machine learning classifiers provided compelling results. The Random Forest classifier exhibited a commendable accuracy of approximately 84%, showcasing its effectiveness in hydration classification. However, the XGBoost classifier surpassed this performance, achieving an accuracy of around 94%. Detailed class-wise metrics demonstrated the superior precision, recall, and F1-scores of both classifiers, emphasizing their proficiency in discerning hydration states.

Random Forest Classifier Results (Table 3): Fully Hydrated Class: The precision is relatively low (0.70), indicating that when the model predicts a sample to be fully hydrated, it might have a higher chance of false positives. However, the recall is high (0.94), suggesting that the model effectively captures the majority of actual fully hydrated instances. The F1-Score, which balances precision and recall, is moderate (0.80). Mid-Hydrated Class: High precision (0.92) indicates that when the model predicts a sample as mid-hydrated, it is likely to be correct. However, the recall is comparatively lower (0.80), meaning that the model may miss some actual mid-hydrated instances. The F1-Score is reasonable at 0.85, reflecting a balance between precision and recall. Dehydrated Class: The model performs well in predicting dehydrated instances, as indicated by high precision (0.96) and moderate recall (0.78). The F1-Score is good at 0.86, suggesting a harmonious trade-off between precision and recall.

XGBoost Classifier Results (Table 4): Dehydrated Class: The precision, recall, and F1-Score for the dehydrated class are all high (0.96, 0.95, 0.95, respectively), indicating that the XGBoost model effectively identifies dehydrated instances with a good balance between precision and recall. Fully Hydrated Class: Similarly, for the fully hydrated class, the XGBoost model demonstrates high precision (0.93), recall (0.96), and F1-Score (0.94), suggesting strong performance in identifying fully hydrated instances. Mid-Hydrated Class: Consistent with the other classes, the XGBoost model performs well for the mid-hydrated class, with high precision (0.96), recall (0.95), and F1-Score (0.95).

Additionally, the cross-validation of the Random Forest classifier illustrated consistent accuracy across five folds, substantiating the model's robustness with a mean accuracy of 83% and a minimal standard deviation of 2%. These findings underscore the reliability and stability of the Random Forest classifier, further solidifying its applicability in practical scenarios. The comprehensive evaluation metrics presented in precision, recall, and F1-scores contribute to a holistic understanding of the classifiers' performance, enriching the insights gained from aggregate analyses.
While a high average training score suggests effective learning, the relatively lower and variable validation scores imply that the model could be sensitive to specific subsets or patterns within the data. It's essential to strike a balance between achieving high accuracy on the training set and ensuring good generalization to new data.

Figure 21 shows the difference between the training and validation accuracy before and after applying Euler Magnification. We notice that Euler Magnification not only improved the training to validation ratio: 5% compared to 16% before applying EVM, but it also slightly improved the accuracy of the overall model from 80% to 84% using less complex parameters

(maximum depth and number of estimators). Our last model operates with a number of estimators of 80 with a maximum depth limit of 5 while the previous model (without EVM) used 100 and 10 respectively.

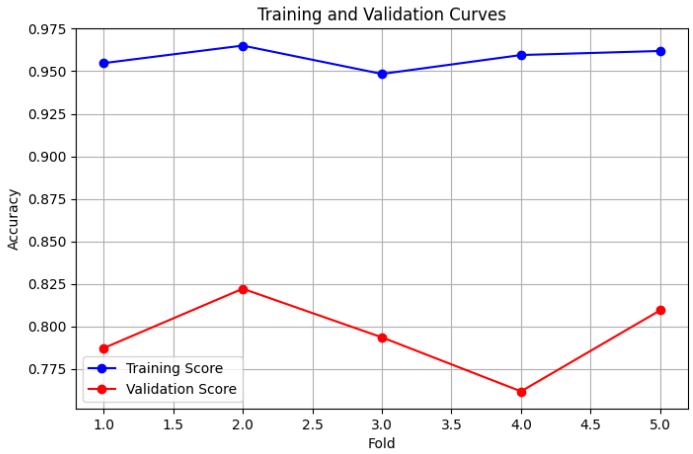

((a)) Before EVM

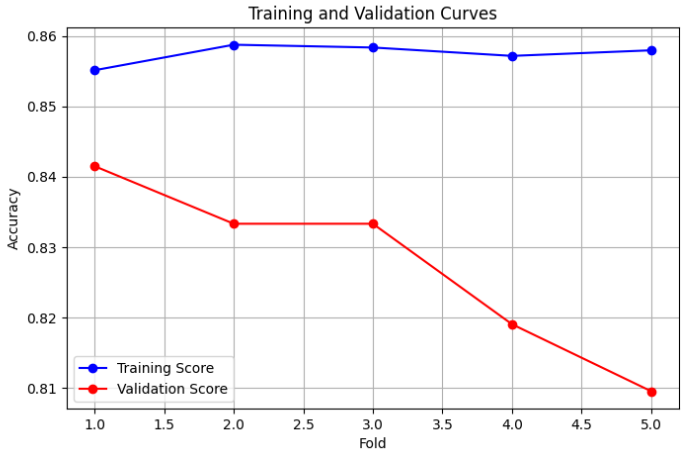

((b)) After EVM

Figure 21: Training vs Validation Accuracy before and after EVM

For individual analyses, the Random Forest model demonstrated an average accuracy of 84%, while the XGBoost model surpassed this, averaging at 90%. These outcomes underscore the superior performance of the XGBoost classifier in discerning hydration states on an individual level. The overall success of both models emphasizes the viability of machine learning for individualized hydration monitoring, yet the nuances in accuracy underscore the need for a nuanced understanding of individual responses to the classification models. In the aggregate analyses, the Random Forest classifier achieved an accuracy of approximately 84%, and the XGBoost classifier outperformed it with an accuracy of around 94%. While these accuracies indicate successful hydration classification, the observed discrepancies between training and validation scores emphasize the importance of addressing potential overfitting in the modeling process, urging a balance between complexity and generalizability for optimal classifier performance.

5 Additional Results: Emotion Recognition

We also delve into additional results, focusing on emotion recognition. For this purpose, a dedicated experimental setup is described, involving the use of spectroscopy data for feature extraction, correlation analysis, and the application of a window sliding algorithm to classify emotions as sad or happy.

5.1 Use case 3: Emotion Recognition Experimental setup

In this approach, we endeavored to categorize two emotions, namely happiness and sadness, using data obtained through spectroscopy. While emotions have been previously explored based on physiological data, this is the first attempt to correlate them with light absorbance. Our investigation of existing literature revealed the following distinctions in physiological variances between the target emotions:

Happiness/Positive Affect: This emotional state is typically associated with relatively stable heart rate, moderate skin conductance, and potentially slightly elevated skin temperature.

Sadness: On the other hand, sadness is characterized by a relatively stable or decreased heart rate, lower skin conductance, and possibly a slight decrease in skin temperature.

We propose that our deep skin spectroscopy sensor can provide insights into all these physiological parameters, including heart rate, skin conductance, and skin temperature. We aim to develop an algorithm that leverages these measurements to effectively classify both happiness and sadness based on the light absorbance data.

5.2 Experiment protocol

Our study cohort was constituted of 5 participants, 3 males and 2 females aged between 22 and 32. To elicit the intended emotions, we had the participants view a 6-minute compilation video tailored to each emotion. To induce happiness, we curated a compilation featuring heartwarming moments, including reunions with loved ones, acts of kindness, and expressions of joy and laughter. For the sadness emotion, we selected videos containing emotional scenes from movies or documentaries that portrayed themes of loss, heartbreak, or poignant moments. To ensure the emotions took effect, we excluded the first minute of the measurement.
As previously mentioned, the equation for absorbance (A) is defined as $A = \log10(I0 / I)$, where I0 represents the incident light's intensity, and I stands for the transmitted light's intensity. In our previous experiments, we employed a blank sample measurement to estimate the incident light (I0). In this particular case, we established a 'neutral' emotional state in which we instructed participants to remain still and engage in meditation or clear their thoughts while we collected their 6 minutes of data.

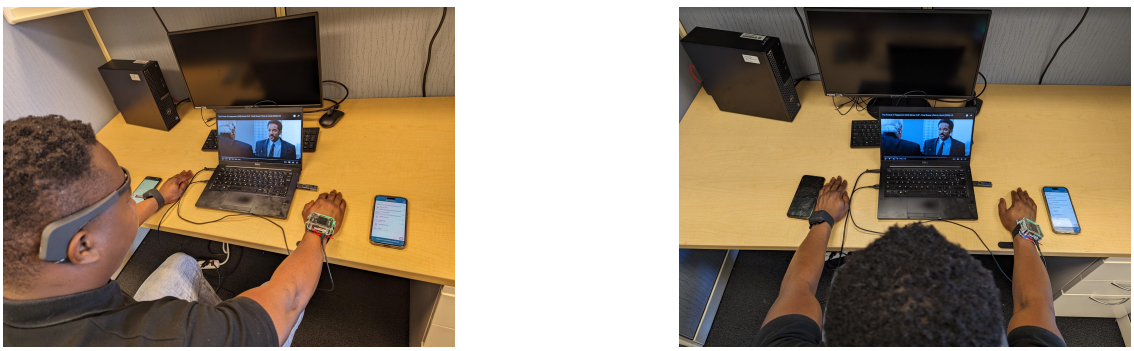

Figure 22: Emotion Recognition Experimental setup

5.3 Using pyEDA for feature extraction on spectroscopy data

We utilized a powerful tool called pyEDA, which is designed for Electrodermal Activity (EDA) analysis, also known as GSR (Galvanic Skin Response). PyEDA v.2.0 is a comprehensive package that encompasses various aspects of EDA data processing and feature extraction. It offers efficient preprocessing of EDA signals and the extraction of pertinent features through a combination of statistical and automated methods. One of the noteworthy functionalities of pyEDA involves the utilization of a Convolutional Autoencoder, a sophisticated technique for automatic feature extraction. The tool provides a wide range of features that can be used for the analysis of EDA data, facilitating the investigation of emotional states. In this experiment, the primary focus was on extracting features from absorbance data captured by the Triad spectroscopy sensor. The specific function employed from pyEDA for this analysis was the "Extract Statistical Features." which generates the following outputs:
Outputs: m: This variable holds measurements for each of the segment indices, including the number of peaks, the mean of EDA, and the maximum value of the peaks. wd: This variable contains filtered phasic GSR, phasic GSR, tonic GSR, and a peaklist for each of the segment indices. eda-clean: This variable stores the preprocessed GSR data, ready for further analysis. graphs and comments.
In our case, after analysing all the results, we noticed that the phasor gsr feature provides very intresting results that would surely permit to distinguish between two emotions, as the figures below shows:

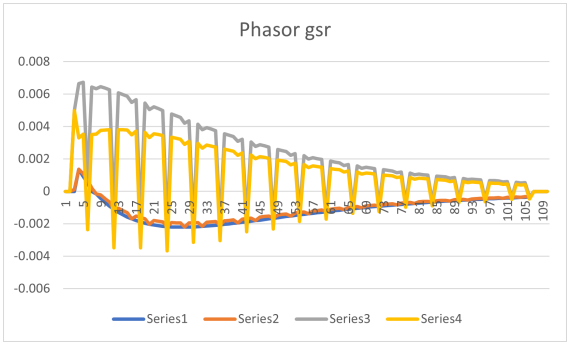

((a)) Participant 1 and 2 Phasor GSR, Series 1 and 2 are Happy state and Series 3 and 4 are Sad

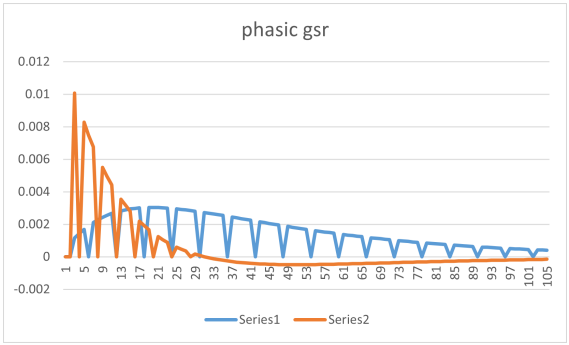

((b)) Participant 3 Phasor GSR, Series 1 is Happy state and Series 2 is Sad

Figure 23: pyEDA feature extraction on participants 1,2 and 3

The data representing the happy state exhibit a distinctive pattern. It begins with a rapid decline from its peak value to a point below zero, then gradually returns to zero, extending

indefinitely. In contrast, the data for the sad state displays a different behavior. It initiates with a peak value and undergoes oscillations, but these oscillations gradually diminish, eventually approaching zero for an infinite duration.

5.4 Correlation Results

Here we generate the cross-correlation matrix similar to our hydration tracking experiment.

In this case we can observe similar patterns in the sad data for every participants, where can clearly see patterns of higher correlations between the channels 0-5 (410nm, 435nm, 470nm, 510nm and 535nm wavelengths) compared to the happy data matrix and a more distributed correlation strength in the rest of the matrix where in the happy data a weaker correlation is observed. Only one exception with participant one where the matrix were a little more similar and the pattern less stressed.

5.5 Window sliding Algorithm to classify sad and happy emotions

In the pursuit of emotion classification, we developed a sliding window algorithm combined with a Random Forest classifier. This approach is designed to leverage spectroscopy data to discern emotional states, specifically happiness and sadness.
We began by loading our preprocessed data, which were organized in separate CSV files representing various emotional states. These data files were harmoniously concatenated into a single dataset, ensuring that the columns aligned correctly. The corresponding labels were then assigned: 1 for happiness, and 2 for sadness.

A critical aspect of our algorithm is the configuration of the sliding window. The sliding window's purpose is to segment the continuous data stream into smaller windows of a specified size. In our case, we determined a window size of 18 measurements, with a step size of 30 measurements. This configuration ensures that each window covers a segment of the data while maintaining overlap to capture transitions and variations in the emotional state.

The sliding window function was implemented to extract these windows and their corresponding labels from the continuous data stream. As the window slides along the data, it collects a set of consecutive measurements and associates them with a label representative of the emotion observed within the window. These windows and labels form the basis for our training and testing datasets.
To train and evaluate the performance of our emotion classification model, the collected windows and labels were divided into training and testing sets. An 80-20 split was employed, with 80% of the data used for training and the remaining 20% for testing.
We chose to employ a Random Forest classifier with 100 trees. This model was trained on the flattened window data obtained from our training set. After training the Random Forest classifier, we applied it to the test data to predict emotional states within the sliding windows. The predictions were then compared to the actual labels to evaluate the model's performance. We calculated the accuracy of the model, and notably, our classifier achieved an accuracy of 83%, signifying its effectiveness in distinguishing between happiness and sadness based on the spectroscopy data captured within the sliding windows. This sliding window algorithm, in conjunction with the Random Forest classifier, demonstrates its potential to effectively classify emotions in real-time based on spectroscopic data, providing a valuable tool for emotion analysis and research.

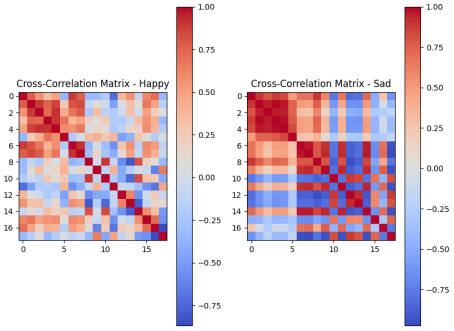

((a)) Participant 1 Happy/Sad Correlation Matrix

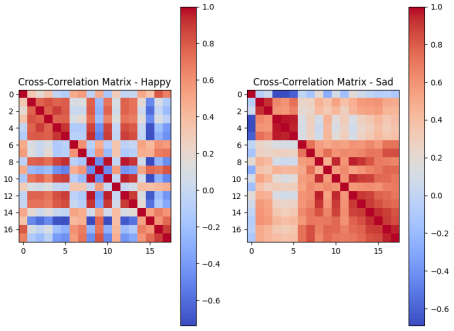

((b)) Participant 2 Happy/Sad Correlation Matrix

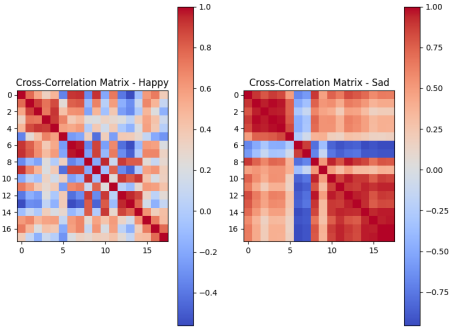

((c)) Participant 3 Happy/Sad Correlation Matrix

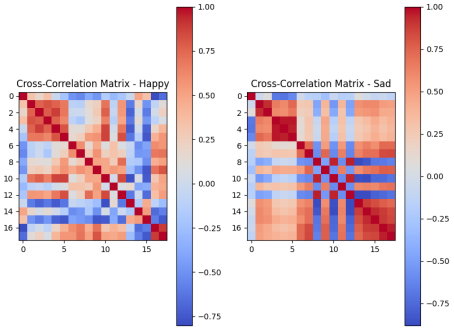

((d)) Participant 4 Happy/Sad Correlation Matrix

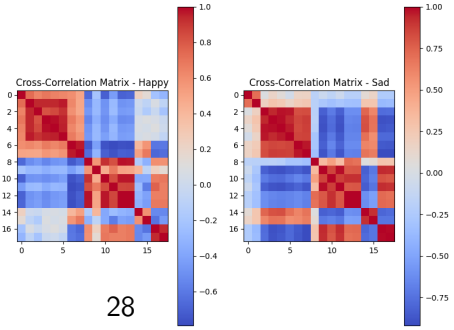

((e)) Participant 5 Happy/Sad Correlation Matrix

Figure 24: Happy/Sad Correlation Matrix

6 conclusion

In this thesis, we have introduced a groundbreaking approach to real-time hydration assessment using a smartwatche equipped with a low-cost spectroscopy sensor. By seamlessly integrating this technology into an everyday wearable, we aimed to offer a convenient and non-invasive method for monitoring hydration levels based on blood electrolyte concentration. Two significant use cases were explored: the measurement of electrolyte solutions and the assessment of skin hydration during workouts and fasting experiments. These use cases demonstrated the credibility of our proposed system.

We presented signal processing techniques for extracting meaningful data from spectroscopic measurements and implemented an AI algorithm on the edge for real-time hydration status classification. The results evaluation showcased the system's accuracy and performance, emphasizing the potential applications in diverse areas of health monitoring. Our study made distinctive contributions by seamlessly incorporating an affordable spectrophotometer into an open-source smartwatch, providing on-device data analytics, and exploring the correlation between emotions and light absorbance—a novel endeavor connecting emotional states with physiological data.

The aggregate analyses, exploring cross-correlation matrices and wavelet transform heatmaps, revealed nuanced variations among hydration states. Machine learning classifiers, particularly the Random Forest and XGBoost, exhibited commendable accuracies, with the latter surpassing the former. The detailed class-wise metrics enriched our understanding of classifier performance. While the Random Forest classifier demonstrated consistency in cross-validation, the slight variation in validation scores suggested the need for further refinement to balance complexity and generalizability.

Additionally, our foray into emotion recognition showcased the effectiveness of a sliding window algorithm combined with a Random Forest classifier. Achieving an accuracy of 83%, this algorithm demonstrated the potential for real-time emotion classification based on spectroscopic data, adding a valuable dimension to emotion analysis and research.

In conclusion, our work contributes significantly to the field of continuous health monitoring, offering a reliable and non-invasive solution for real-time hydration assessment. The findings underscore the potential of wearable biosensors in health monitoring and pave the way for future research and refinement of the proposed technology.

7 Future Work

- Following this successful proof of concept, our next step involves undertaking comprehensive clinical trials. These trials will involve benchmarking our hydration classification model against established and accurate hydration tracking devices, such as the MX3 Hydration Testing System (https://www.mx3diagnostics.com/products/hydration-testing-system-pro).

- To enhance the precision of our hydration tracking system, a crucial step is the explicit definition of hydration biomarkers. This entails a meticulous examination and selection of specific electrolytes or wavelengths absorbance that serve as reliable indicators of hydration status.

- Recognizing the pivotal role of data quantity in refining machine learning models, our strategy involves an expansive data collection initiative. By amassing a more extensive dataset, we aim to fortify the robustness and generalizability of our machine learning model for improved hydration classification.

- Acknowledging the sensitivity of the sensor to motion, we implemented strict measures during data collection, urging participants to remain still. Looking forward, we plan to integrate a gyroscope into the sensor system. This addition will enable the detection of motion noise, subsequently facilitating the implementation of a motion artifact removal algorithm. This advancement is pivotal in ensuring the accuracy and reliability of our hydration tracking system, especially in real-world scenarios where participant movement is inevitable.

- Broaden the scope of the emotion recognition study to encompass additional classes, including fear, excitement, disgust, anger, and others.

References

[1] D. C. Garrett, N. Rae, J. R. Fletcher, S. Zarnke, S. Thorson, D. B. Hogan, and E. C. Fear. Engineering approaches to assessing hydration status. *IEEE Reviews in Biomedical Engineering*, 11:233–248, 2018.

[2] I. M. Gidado, M. Qassem, I. F. Triantis, and P. A. Kyriacou. Review of advances in the measurement of skin hydration based on sensing of optical and electrical tissue properties. *Sensors*, 22(19):7151, 2022.

[3] M. Qassem and P. Kyriacou. Review of modern techniques for the assessment of skin hydration. *Cosmetics*, 6(1):19, 2019.

[4] Y. Hao and R. Foster. Wireless body sensor networks for health-monitoring applications. *Physiological Measurement*, 29(11):R27–R56, 2008.

[5] Iman M. Gidado, Meha Qassem, Iasonas F. Triantis, and Panicos A. Kyriacou. Review of advances in the measurement of skin hydration based on sensing of optical and electrical tissue properties. *Sensors*, 22(19), 2022.

[6] Yarden Tzabari Kelman, Sagie Asraf, Nisan Ozana, Nadav Shabairou, and Zeev Zalevsky. Optical tissue probing: human skin hydration detection by speckle patterns analysis. *Biomedical Optics Express*, 10, 2019.

[7] Ian Butterworth, Jose Seralles, Carlos S. Mendoza, Luca Giancardo, and Luca Daniel. A wearable physiological hydration monitoring wristband through multi-path non-contact dielectric spectroscopy in the microwave range. 2015.

[8] Noelle R. Benavides, Hayley E. Rutkey, Courteney M. Didomenico, Tin Wong, Joe Martel-Foley, Chen Hsiang Yu, and Ali Kiapour. A wearable mobile-app controlled device for continuous monitoring of uv exposure and hydration levels. 2021.

[9] Vincenzo F. Curto, S. Coyle, R. Byrne, D. Diamond, and F. Benito-Lopez. Real-time sweat analysis: Concept and development of an autonomous wearable micro-fluidic platform. volume 25, 2011.

[10] Emre O. Polat, Gabriel Mercier, Ivan Nikitskiy, Eric Puma, Teresa Galan, Shuchi Gupta, Marc Montagut, Juan José Piqueras, Maryse Bouwens, Turgut Durduran, Gerasimos Konstantatos, Stijn Goossens, and Frank Koppens. Flexible graphene photodetectors for wearable fitness monitoring. *Science Advances*, 5, 2019.

[11] Nisan Ozana, Nadav Arbel, Yevgeny Beiderman, Vicente Mico, Martin Sanz, Javier Garcia, Arun Anand, Baharam Javidi, Yoram Epstein, and Zeev Zalevsky. Improved noncontact optical sensor for detection of glucose concentration and indication of dehydration level. *Biomedical Optics Express*, 5, 2014.

[12] Vicki Sandys, Colin Edwards, Paul McAleese, Emer O'Hare, and Conall O'Seaghdha. Protocol of a pilot-scale, single-arm, observational study to assess the utility and acceptability of a wearable hydration monitor in haemodialysis patients. *Pilot and Feasibility Studies*, 8, 2022.

[13] Mohammad Mamouei, Subhasri Chatterjee, Meysam Razban, Meha Qassem, and Panayiotis A. Kyriacou. Design and analysis of a continuous and non-invasive multi-wavelength optical sensor for measurement of dermal water content. *Sensors*, 21, 2021.

[14] M. Mamouei, M. Qassem, M. Razban, and P. A. Kyriacou. Measurement of dermal water content using a multi-wavelength optical sensor. volume 2020-July, 2020.

[15] M. Qassem and P. A. Kyriacou. In vivo optical investigation of short term skin water contact and moisturizer application using nir spectroscopy. 2013.

[16] Ariel Bohman, John Q. Nguyen, Sanjana Parthasarathy, and Mark A. Arnold. Temperature and hydration monitoring in tissue-simulating phantoms using novel silicon-photonics-based spectrophotometer. 2023.

[17] Robbe Van Beers, Michael Jacobs, Alex Borgoo, Miek Hornikx, Stefan Janssens, Ward van der Tempel, and Jonathan Borremans. Accurate measurement of spo2 and dermal skin hydration using a wearable miniaturized spectrometer. 2022.

[18] Hidenobu Arimoto and Mariko Egawa. Non-contact skin moisture measurement based on near-infrared spectroscopy. *Applied Spectroscopy*, 58, 2004.

[19] Rockley. Bioptx™ biosensing band. `https://rockleyphotonics.com/bioptx-band/`, 2023. Accessed on 15 July 2023.

[20] Sixty. Sixty hydration monitor. `https://sixty.ie`, 2023. Accessed on 15 July 2023.

[21] BSX Athletics. Lvl-the first wearable hydration monitor. `https://www.kickstarter.com/projects/lactate-threshold/lvl-the-first-wearable-hydration-monitor`, 2023. Accessed on 15 July 2023.

[22] hDrop Technologies Inc. hdrop-electrolytes, hydration, and temperature tracker. `https://www.kickstarter.com/projects/hdrop/hdrop-real-time-hydration-wearable-device-monitor?ref=cqtb72`, 2023. Accessed on 15 July 2023.

[23] Hydrostasis. real-time hydration monitoring. `https://www.hydrostasis.com/#intro`, 2023. Accessed on 15 July 2023.

[24] Apple. Patently apple. `https://www.patentlyapple.com/2021/08/one-of-the-next-health-features-that-may-be-coming-to-apple-watch-relates-to-trackin` `html`, 2023. Accessed on 15 July 2023.

[25] Epicore Biosystems. Continuous real-time hydration monitoring. `https://www.epicorebiosystems.com/connected-hydration/`, 2023. Accessed on 15 July 2023.

[26] Nix. Nix biosensors. `https://nixbiosensors.com`, 2023. Accessed on 15 July 2023.

[27] Pinar Avci, Asheesh Gupta, Magesh Sadasivam, Daniela Vecchio, Zeev Pam, Nadav Pam, and Michael Hamblin. Low-level laser (light) therapy (lllt) in skin: stimulating, healing, restoring. *Seminars in cutaneous medicine and surgery*, 32:41–52, 03 2013.

[28] SparkFun Electronics. Sparkfun triad spectroscopy sensor - as7265x (qwiic). `https://www.sparkfun.com/products/15050`, 2023. Accessed on 10 May 2023.

[29] Hach. Dr3900 laboratory spectrophotometer for water analysis. `https://www.hach.com/p-dr3900-laboratory-vis-spectrophotometer-with-rfid-technology/LPV440.99.00012`, 2023. Accessed on 10 May 2023.

[30] DSTIKE. Dstike deauther watch v4. https://dstike.com/products/dstike-deauther-watch-v4s, 2023. Accessed on 10 May 2023.

[31] Hao-Yu Wu, Michael Rubinstein, Eugene Shih, John Guttag, Frédo Durand, and William T. Freeman. Eulerian video magnification for revealing subtle changes in the world. *ACM Transactions on Graphics (Proc. SIGGRAPH 2012)*, 31(4), 2012.

[32] Yeting Guo, Fang Liu, Zhiping Cai, Li Chen, and Nong Xiao. FEEL: A federated edge learning system for efficient and privacy-preserving mobile healthcare. In *49th International Conference on Parallel Processing - ICPP*, New York, NY, USA, August 2020. ACM.

[33] Partha Pratim Ray. A review on tinyml: State-of-the-art and prospects. *Journal of King Saud University - Computer and Information Sciences*, 34, 2022.

[34] Lachit Dutta and Swapna Bharali. Tinyml meets iot: A comprehensive survey. *Internet of Things (Netherlands)*, 16, 2021.